



Optimal siting, sizing and control of battery energy storage to enhance dynamic stability of low-inertia grids

Jannesar, Mohammad Rasol; Sadr, Sajad; Savaghebi, Mehdi

Published in:
IET Renewable Power Generation

Link to article, DOI:
[10.1049/rpg2.13079](https://doi.org/10.1049/rpg2.13079)

Publication date:
2024

Document Version
Publisher's PDF, also known as Version of record

[Link back to DTU Orbit](#)

Citation (APA):
Jannesar, M. R., Sadr, S., & Savaghebi, M. (2024). Optimal siting, sizing and control of battery energy storage to enhance dynamic stability of low-inertia grids. *IET Renewable Power Generation*, 18(15), 2925-2941.
<https://doi.org/10.1049/rpg2.13079>

General rights

Copyright and moral rights for the publications made accessible in the public portal are retained by the authors and/or other copyright owners and it is a condition of accessing publications that users recognise and abide by the legal requirements associated with these rights.

- Users may download and print one copy of any publication from the public portal for the purpose of private study or research.
- You may not further distribute the material or use it for any profit-making activity or commercial gain
- You may freely distribute the URL identifying the publication in the public portal

If you believe that this document breaches copyright please contact us providing details, and we will remove access to the work immediately and investigate your claim.

Optimal siting, sizing and control of battery energy storage to enhance dynamic stability of low-inertia grids

Mohammad Rasol Jannesar¹  | Sajad Sadr² | Mehdi Savaghebi³ 

¹Department of Electrical Engineering, Technical and Vocational University (TVU), Tehran, Iran

²Department of Electrical Engineering, Tafresh University, Tafresh, Iran

³Department of Engineering Technology, Technical University of Denmark (DTU), Ballerup, Denmark

Correspondence

Sajad Sadr, Department of Electrical Engineering, Tafresh University, Tafresh, Iran.

Email: sadr@tafshu.ac.ir

Abstract

As inverter-based resources like wind turbines increase, grid inertia and stability decrease. Optimal placement and control of energy storage systems can stabilise low-inertia grids. This paper investigates how optimal battery energy storage systems (BESS) enhance stability in low-inertia grids after sudden generation loss. The sitting, sizing and control of BESS are determined simultaneously in each genetic algorithm (GA) population, then voltage and frequency stability is evaluated based on the network simulation. This continues until the optimal solution is found. A network based on Kundur's four-machine system is modelled for the first study and two of the four synchronous generators (SGs) have been replaced with wind farms. Then, the production of the third SG has been decreased by 13%. According to the results, addition of wind farms causes the frequency drop below 49.6 Hz for more than 5 min, indicating instability. It is also demonstrated that with optimal control parameters and placement, a 60 MW BESS can alleviate the voltage and frequency fluctuations, leading to enhanced stability. This method has also been tested on the IEEE 39-bus network, where the installation of a BESS with a capacity of 9 MVA could restore the frequency stability.

1 | INTRODUCTION

1.1 | Problem statement

More utilization of renewable energy sources (RESs) can considerably reduce the air pollution and the rate of global warming [1]. Furthermore, thanks to technology developments in manufacturing of wind turbines (WTs) and photovoltaic (PV) systems, the cost of these systems is reduced to the levels even cheaper than conventional power plants [2]. Therefore, technical, environmental, and economic factors motivate increased utilization of RESs [3], as presented in Figure 1. On the other hand, proliferation of RESs can lead to issues such as degraded stability, intermittent power, challenges in active and reactive power control, etc. [4]. Low inertia is another impact of RESs integration that has two consequences on the frequency stability including high rate of change of frequency (RoCoF) and frequency nadir which results in trip of relays and a high-unintentional load shedding, respectively [5]. Optimal location, sizing, and control of energy storage systems can improve stability in low-inertia grid.

1.2 | Literature review

Classical categorization of power system stability is mentioned in many references such as [6–8] which can be summarized as voltage, frequency and rotor angle stability. As we know, the base of power system frequency is synchronous generator (SG) rotor speed. These rotors, thanks to their weight and moment of inertia, contribute to damping the system disturbances. Proliferation of RESs leads to the reduction of conventional SGs' share in power systems. Furthermore, RESs are mostly connected to grid by power electronic converters. Thus, power system inertia decreased with increased share of RESs in power generation [5, 9–12]. This is a big challenge for system stability, especially in terms of frequency fluctuations.

Different uses of energy storage systems (ESSs) in the network include bulk energy, ancillary, renewable energy integration, and customer management services which frequency control is a subset of ancillary services [13]. The methods for frequency control in presence of RESs can be categorized as techniques with and without ESS for solar PV plant and WT [12]. As discussed in that paper frequency control

This is an open access article under the terms of the [Creative Commons Attribution-NonCommercial-NoDerivs](#) License, which permits use and distribution in any medium, provided the original work is properly cited, the use is non-commercial and no modifications or adaptations are made.

© 2024 The Author(s). *IET Renewable Power Generation* published by John Wiley & Sons Ltd on behalf of The Institution of Engineering and Technology.

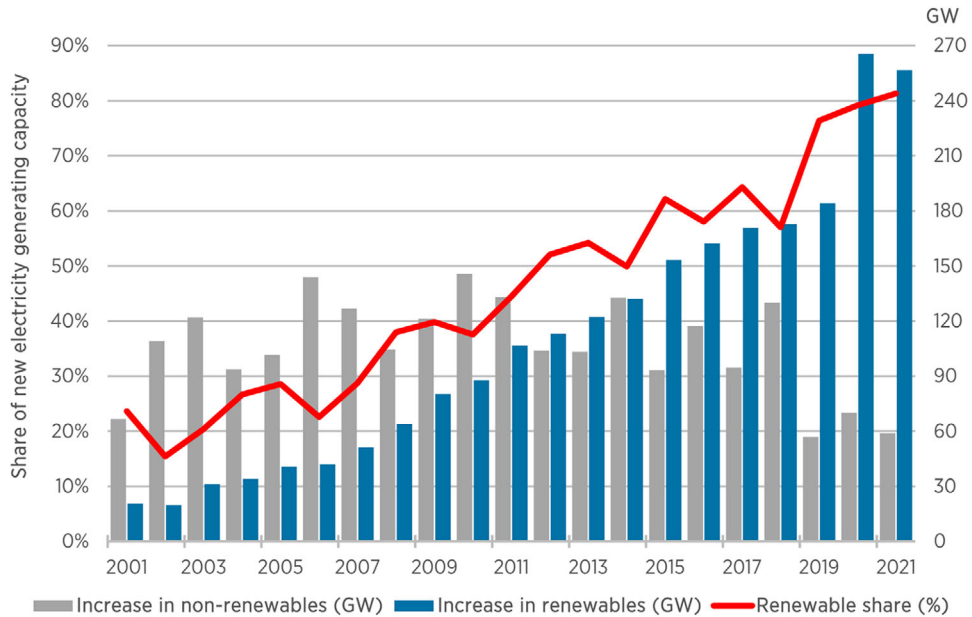


FIGURE 1 Trend of intensity to utilization of renewable energy resources in the last two decades [3].

techniques without ESS have different types that is, solar PV plant; de-loading technique, techniques for WT consist of: (1) inertial response involves hidden inertia emulation and fast power reserve, (2) droop control, and (3) de-loading that involves over speed control and pitch angle control. While frequency control techniques with ESS have only two types, that is, techniques for solar PV plant and WT. So, frequency control techniques without ESS are developed more than with ESS. Hence, the focus of this paper is on frequency control techniques with ESS.

One of the main ESS technologies applied in the electricity grid is battery energy storage system (BESS). BESS in power system can play different roles such as smoothing the generated WT like [14], power system peak shaving like [15] and improving the frequency stability like [16–18], which the third mentioned application is the goal of this paper.

In [11], improving frequency stability by synchronous compensators and BESS for a small power system, that is, Sardinia Island is investigated. They used a new equivalent saturation logic to adjust the BESS control. Refer to their results, up to 50% decrease in inertia, that system has an accepted performance for both under-frequency and over-frequency situations. A case study for the role of BESS to improve power system stability in Sri Lanka is reported in [19]. In that research, they installed BESS and superconductors at load centres. In under-frequency situation by injecting the active power, load shedding can be prevented, and recovery time is reduced. In over-frequency by absorbing the active power, system stability can be improved. One of the main factors for improving power system stability using this approach is the proper location (optimal siting) of the ESS, which is discussed in [18]. As their results of simulation on a 16 machine 68 bus system, for primary frequency response if the RES penetration is low, the place of ESS does not have important effect, while when the RES

penetration is high, the importance of ESS location significantly increases.

1.3 | Research gap

In [20], by considering a low-inertia power grid facing loss of generation, the effect of BESS on stability enhancement is evaluated but no optimisation has been performed on location, size, and control parameters of BESS. In [21], optimal sizing and placement of BESS is performed to improve frequency stability while sizing and siting are not simultaneously. In other words, first, the optimal size of the BESS is determined, and then with another optimization according to the determined size, the optimal location is performed. Optimal placement and sizing of BESS is carried out in [22] for frequency and voltage stability without optimizing the BESS control parameters. In the present paper, the stability of both frequency and voltage is improved by optimal and siting, sizing, and setting of control parameters of BESS in a low-inertia grid with different penetration levels of renewable energy.

1.4 | Contribution

The contribution of current paper can be presented as

- Simultaneous optimization of size, location, and control parameters of BESS for enhanced stability of power grid.
- Optimization for minimized rating of BESS and RoCoF and maximized frequency nadir.

The rest of the paper is organized as follows. Section 2 describes the WT and BESS modelling and control. Optimal

siting, sizing, and control of BESS is proposed in Section 3. Section 4 is dedicated to the simulation results and analysis. Finally, Section 5 outlines the main findings to conclude the paper.

2 | MODELLING AND CONTROL OF WT AND BESS

As mentioned earlier, with the appearance of RES such as WT and the replacement of SGs with these sources, the inertia of the network is reduced and the network is associated with voltage and frequency stability problems. One of the available solution is to use BESS. Therefore, in this section, appropriate modelling of SG, WT and BESS is discussed.

2.1 | SG modelling

This paper uses a SG model with no droop in PowerFactory. In Figure 2, the block diagram of SG is illustrated [23]. As it can be seen, the output power, terminal voltage, and speed of SG are entered in the power stabilizer (PSS) and the output of PSS, voltage reference, and terminal voltage are considered as input of automatic voltage regulator (AVR) exciter. The output of AVR is the first input of SG block. The governor and turbine provide the second input by considering the deference between reference and network frequency. The details of modelling the governor and AVR are provided in the appendix by Figures A1 and A2, respectively [24].

2.2 | WT modelling

This paper uses WT to model a wind farm and also a fully-rated converter (FRC) model, which is more common in new designs, especially in recent high-power WTs. The block diagram of Figure 3 depicts the WT model [25]. As it can be seen, firstly, the voltage, current and active and reactive powers are measured from the point of common coupling (PCC) of the WT, and $\sin(\theta_{\text{ref}})$ and $\cos(\theta_{\text{ref}})$ are calculated by the phase-locked loop (PLL). The measured active and reactive

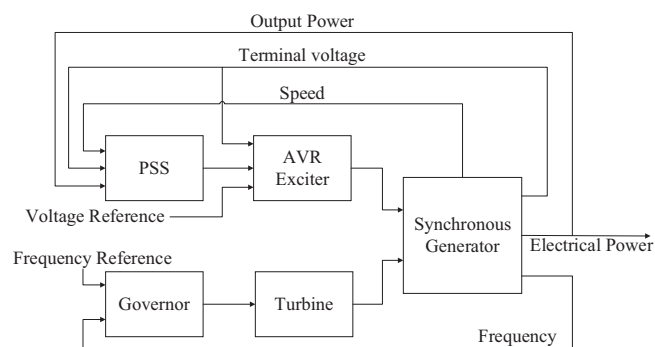


FIGURE 2 Synchronous generator model. AVR, automatic voltage regulator; PSS, power stabilizer.

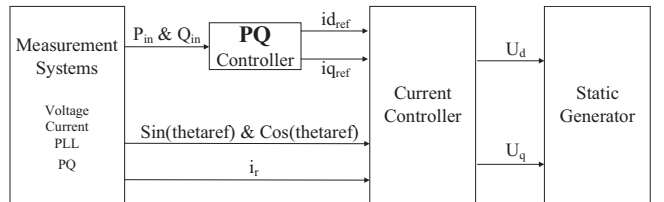


FIGURE 3 Wind turbine model. PLL, phase-locked loop.

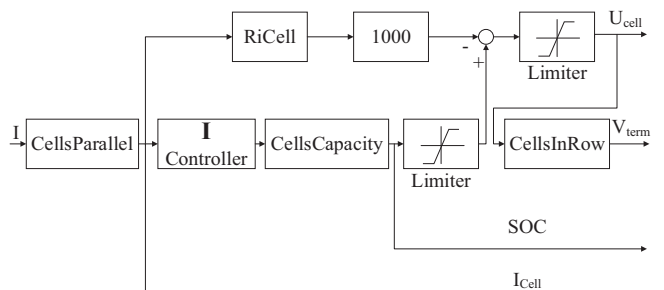


FIGURE 4 Battery energy storage system model. SOC, state of charge.

TABLE 1 Parameters of battery energy storage system model.

Variable	Description	Parameter	Unit
SOC ₀	State of charge (SOC) at initialization	80	%
CellsCapacity	Capacity per cell	80	Ah
CellsParallel	Number of parallel cells	60	—
CellsInRow	Number of cells in row	65	—
RiCell	Intern Resistance per cell	0.001	Ω

power values (P_{in} and Q_{in}) are entered into the PQ control block and create reference dq -current ($i_{d\text{ref}}$ and $i_{q\text{ref}}$). These dq -current along with $\sin(\theta_{\text{ref}})$, $\cos(\theta_{\text{ref}})$ and the real component of current (i_r) by entering the current controller block produce dq -voltages (U_d and U_q) which are the input of the WT generator block diagram. The details of modelling PQ and current controllers are provided in the appendix by Figures A3 and A4, respectively [24].

2.3 | BESS modelling

In Figure 4, the block diagram for BESS modelling is expanded [26]. The description and value for variables of Figure 3 are provided in Table 1.

The state of charge (SOC) is calculated with an integrator, counting the current of the BESS

$$U_{\text{DC}} = U_{\max} \cdot \text{SOC} + U_{\min} \cdot (1 - \text{SOC}) - I \cdot Z_i \quad (1)$$

where U_{\min} and U_{\max} are voltage of discharged and fully charged cell, respectively. Also, I is the discharge current and Z_i is inner resistance [26].

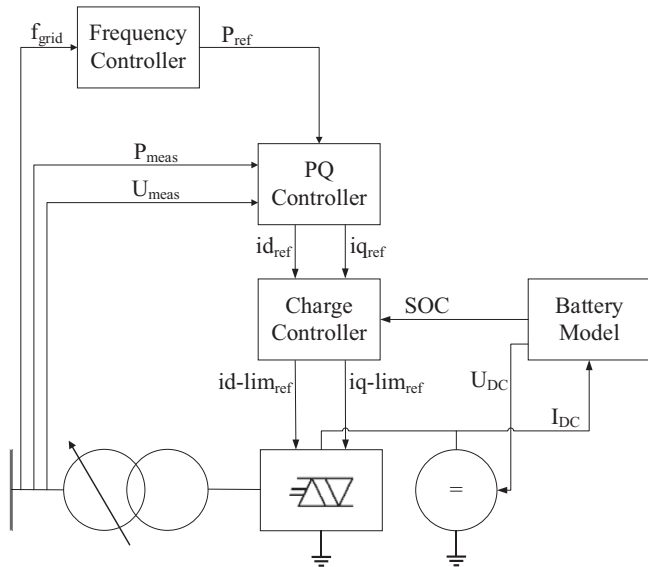


FIGURE 5 Battery energy storage systems controller [27]. SOC, state of charge.

2.4 | BESS control

In BESS controller, d -axis and q -axis are two current parameters that should be controlled. The d -axis and q -axis components control active and reactive power, respectively. With the active and reactive power, the frequency and voltage could be controlled, respectively. In Figure 5, the block diagram for BESS controller is introduced [27]. As can be seen in this figure, the frequency, power, and voltage of the network are measured. The frequency of the network is entered into the frequency controller block and makes the reference power. The reference power along with the measured power and voltage is entered into the PQ controller block and produces the reference current of the dq -frame. These currents produce reference limited dq -currents according to the SOC in the charge controller block, which are given to the inverter.

The whole controller (Figure 5) can be divided into smaller parts such as PQ, charge, and frequency controller shown in Figures 6–8. Figure 6 presents the block diagram for PQ controller which is described in [26]. As can be seen, the difference between the measurement power and the reference power is given to a low-pass filter and then the output of that is added to Δi that is the difference between id_{ref} and $Id-lim_{ref}$ (see Figure 7). This signal is fed to a PI controller and its output after passing through the limiter makes the id_{ref} . On the other hand, the difference between the measurement and the reference voltage (respectively U_{meas} and V_{ref}) after passing through the low-pass filter is fed to I controller and Dead Band blocks. The sum of the outputs of these blocks makes the iq_{ref} .

In Figure 7, the block diagram for charge controller is shown [26]. As it can be seen, Id_{ref} and SOC are fed to the current controller, and the output of this controller along with the iq_{ref} and U_{ac} pass through the current limiter block. The output of this block makes the $Id-lim_{ref}$ and $Iq-lim_{ref}$.

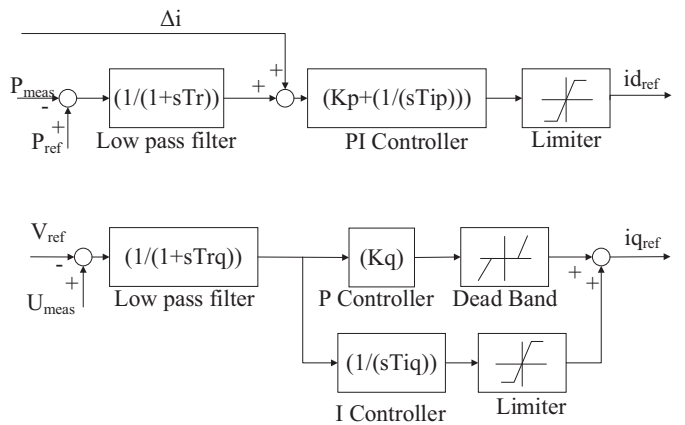


FIGURE 6 PQ controller.

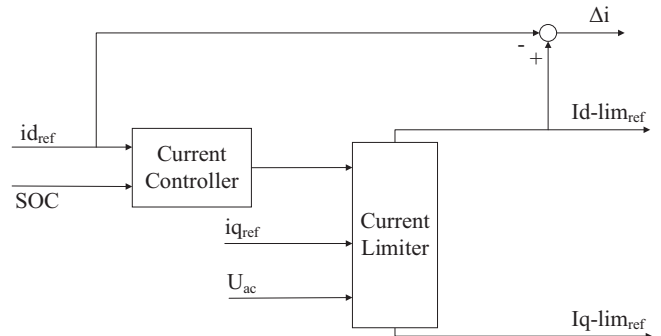


FIGURE 7 Charge controller. SOC, state of charge.

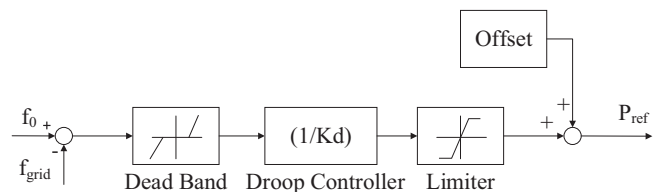


FIGURE 8 Frequency controller.

Figure 8 shows the block diagram of the frequency controller as detailed in [26]. First, the frequency difference is given to the Dead Band block and after passing through the droop controller and the limiter, it is added with the offset value to generate the reference power P_{ref} .

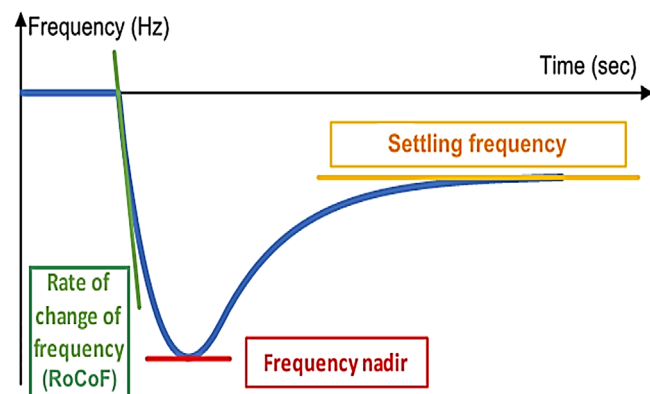
3 | OPTIMAL SITTING, SIZING, AND CONTROL

Frequency stability is the ability of a power system to maintain system frequency within the determined operating limits. Frequency instability is a result of a significant imbalance between load and generation.

According to the operating instructions of Iran's electricity network, the tolerable duration and necessary measures for

TABLE 2 Operating instructions.

	Ranges	Tolerable duration	Necessary measures
Frequency (Hz)	$49.8 < f < 50.2$	Unlimited	Without measures
	$49.6 < f < 49.8$	5 min	Should be returned to $49.8 < f < 50$
	$49.4 < f < 49.6$	5 min	Should be returned to $49.8 < f < 50$
	$50.2 < f < 50.5$	5 min	Should be returned to $50 < f < 50.2$
	$f > 50.5$	3 min	Should be returned to $50 < f < 50.2$
	$f < 49.4$	3 min	Should be returned to $49.8 < f < 50$
Voltage (%)	$-2\% < V < +2\%$	Unlimited	Without measures
	$-10\% < V < -2\%$	5 min	Should be returned to $-2\% < V < +2\%$
	$+2\% < V < +5\%$		
	$V < -10\%$	Intolerable	Should be returned to $-2\% < V < +2\%$
	$V > +5\%$		

**FIGURE 9** Illustration of rate of change of frequency and frequency nadir [31].

different frequency and voltage ranges are as Table 2 [28]. According to Table 2 standard range for frequency and voltage is ± 0.2 Hz and $\pm 2\%$, respectively. In addition, the ranges of $49.4 < f < 49.8$ and $50.2 < f < 50.5$ can be tolerated for 5 min and should be returned to ± 0.2 Hz. Also, the ranges of $f > 50.5$ and $f < 49.4$ can be tolerated for shorter duration, that is, 3 min and must be returned to ± 0.2 Hz, immediately. About voltage, the ranges of $-10\% < V < -2\%$ and $+2\% < V < +5\%$ can last up to 5 min and then should be returned to $\pm 2\%$. Also, the ranges of $V < -10\%$ and $V > +5\%$ are intolerable and must be returned to $\pm 2\%$, immediately.

Frequency nadir and RoCoF are the most common stability indices used to evaluate the frequency stability of power systems [29, 30] and shown in Figure 9. The frequency nadir is defined as the minimum value of frequency reached during the transient period. RoCoF is the absolute maximum time derivative of the power system frequency (df/dt).

This paper defines RoCoF as

$$\text{RoCoF} = \max \left| \frac{\Delta f}{\Delta t} \right| \quad (2)$$

where Δt is step size of simulation in RMS simulation in PowerFactory which is fixed and equal to 0.01 s. Also Δf is frequency variations. So RoCoF is the absolute maximum Δf to Δt ratio.

In order to optimize the allocation and control of BESS, frequency nadir and RoCoF are considered in the objective function.

3.1 | Objective function

There are three terms in objective function included active power of BESS, RoCoF and frequency nadir. Considering that RoCoF unit is frequency per second and nadir is frequency, in order to make the values of these two terms comparable, the frequency nadir has been rewritten as relative frequency nadir (RFN)

$$\text{RFN} = \left| \frac{50 - \text{Frequency Nadir}}{50} \right| \quad (3)$$

The objective function is expressed as the Equation (4). To increase the stability of the network with minimum BESS capacity, the $[P_{\text{BESS}} + \text{RoCoF}]$ and $[\text{RFN}]$ should respectively be reduced and increased. As a result, assuming that the objective function should be minimized to be optimized, the sign between $[P_{\text{BESS}} + \text{RoCoF}]$ and $[\text{RFN}]$ should be negative.

$$\text{OF} = [P_{\text{BESS}} + \text{RoCoF}] - [\text{RFN}] \quad (4)$$

where P_{BESS} is active power of BESS.

In order to maintenance voltage and frequency in allowable ranges, following constraints are considered

$$0.98 < V^k < 1.02 \quad \forall k \in N_b \quad 49.8 < F^k < \quad \forall k \in N_b \quad (5)$$

where V^k and F^k are voltage in per unit and frequency in Hz of k th bus at steady state after disturbance. Also, N_b is the number of study network buses.

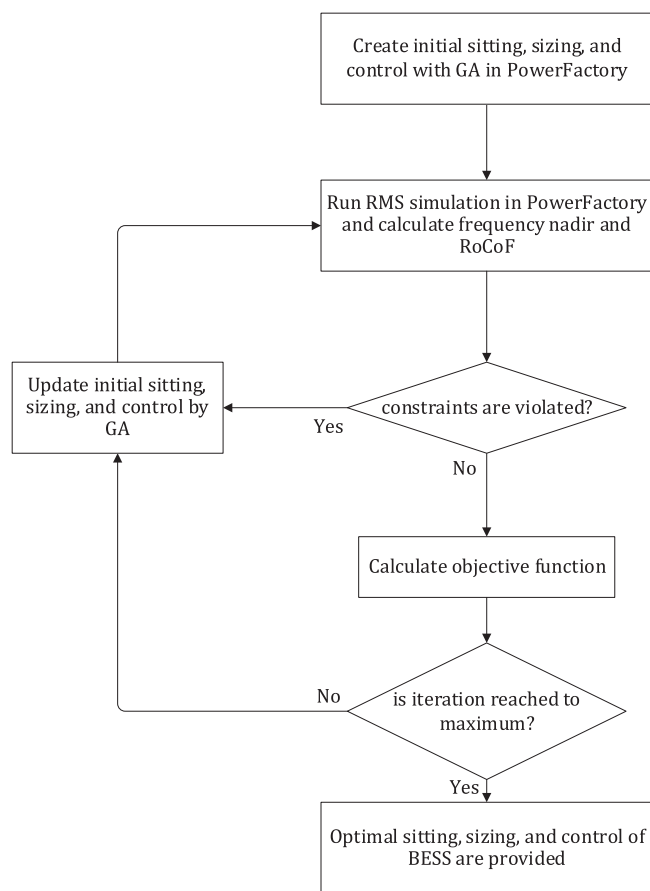
3.2 | Optimization approach

The flowchart of optimization approach is shown in Figure 10. As can be seen, firstly the initial BESS siting, sizing, and control parameters are determined by the genetic algorithm (GA) in PowerFactory. The maximum iterations and population size of GA is equal to 100 and 200, respectively. The format of the GA's gene is shown in Table 3. As it can be seen, by using three chromosomes for the location of the BESS, Buses 5–11 (see Figure 11) are considered as candidates for BESS installation. The BESS size can be selected between 3 and 96 MW. Also, for BESS control parameters, based on values in [22], suitable limits have been adopted according to their acceptable values.

TABLE 3 The format of the gene.

Parameter		Number of Chromosome	Range	Implementation	Unit
BESS sitting	Placement of BESS	3	0–7	Bus 5, 6, 7, 8, 9, 10, and 11 (see Figure 10)	—
BESS sizing	Active power of BESS	5	0–31	$(1, 2, \dots, 32) \times 3$	MW
BESS control	PQ controller	Tr	0–7	$\frac{i}{10^2}$ and $i = 1, 2, \dots, 8$	s
		Trq	0–3	$\frac{1}{10^7}$ and $i = 1, 2, \dots, 4$	s
		Kp	0–127	$1, 2, \dots, 128$	p.u.
		Tip	0–7	$\frac{10}{10^i}$ and $i = 0, 1, \dots, 7$	s
		Kq	0–7	$1, 2, \dots, 8$	p.u.
		Tiq	0–7	$\frac{10}{10^i}$ and $i = 0, 1, \dots, 7$	s
	Frequency Controller	Kd	0–15	$\frac{i}{10^3}$ and $i = 1, 2, \dots, 16$	p.u.
		Dead Band	0–15	$\frac{i}{10^4}$ and $i = 1, 2, \dots, 16$	p.u.

Abbreviation: BESS, battery energy storage systems.

**FIGURE 10** Flowchart of optimization approach. BESS, battery energy storage systems; GA, genetic algorithm; RoCoF, rate of change of frequency.

In the second step, by considering the location, size, and control parameters of BESS from the previous steps, RMS simulation is run in PowerFactory and frequency nadir and RoCoF values are calculated. Then, constraints of voltage magnitude and frequency are evaluated. If the constraints are violated, the ini-

tial calculations are updated by crossover and mutation in each iteration; otherwise, in the fourth step the objective function is calculated. Then, the stop criterion is checked. If the maximum number of iterations is reached, the optimal sitting, sizing and control of BESS are provided.

4 | SIMULATION RESULTS

In this section the optimization approach introduced in Section 3 is implemented for two case studies, that is, Kundur's four-machine and IEEE 39-bus systems. This paper investigates the network dynamic stability under relatively small generation variations without any physical change to the network [32].

4.1 | Kundur's four-machine system

The study network in this case study is a modified Kundur's four-machine system modelled in PowerFactory and can be seen in Figure 11 [33]. In this system, the capacitor C_3 with a capacity of 125 MVar is added to Bus 8 for increasing the bus voltage to a range suitable for the simulation study. The size of SGs, WTs, loads, and capacitors is reported in Table 4.

In order to investigate the effect of increased penetration WTs and addition of optimal BESS on the frequency and voltage stability, four scenarios have been considered as listed in Table 5. In each scenario, the network voltage and frequency are evaluated in the event of 13% decrease in SG₁ production with and without BESS and WT. First, the voltage and frequency of the network are analysed without WT and BESS. To evaluate the impact of RES integration on voltage and frequency stability, in the second and third scenario, one and two WTs are added to the network, respectively. The WTs replace the conventional power plants, that is, SG₂ and SG₄, in the corresponding bus (see Figure 11). In the fourth scenario the improvement of voltage and frequency fluctuation as a result of integrating optimal BESS is demonstrated.

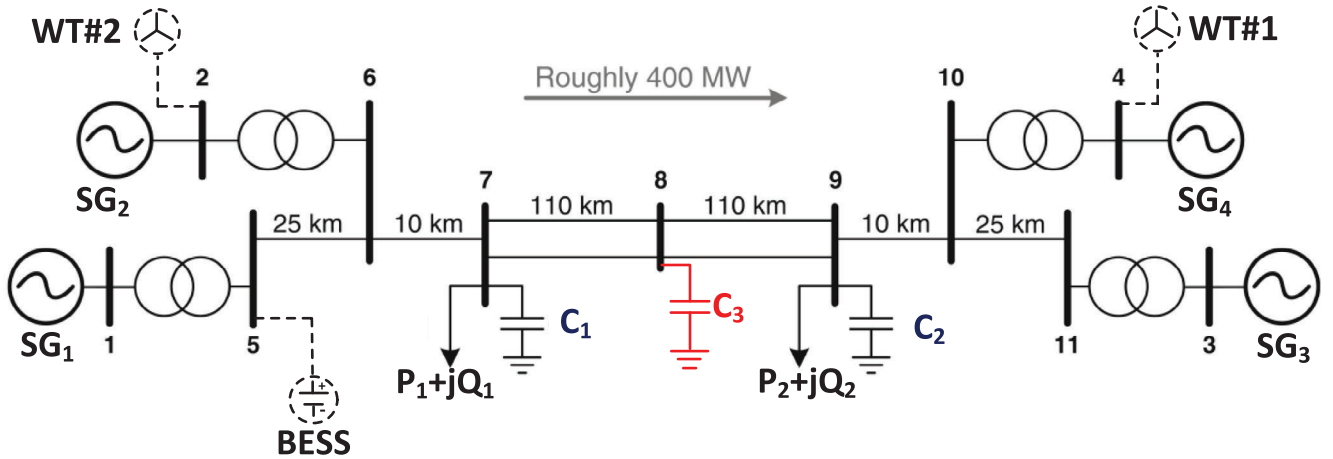


FIGURE 11 Modified Kundur's four-machine system. WT, wind turbine.

TABLE 4 Power ratings of network components.

Bus	P_G (MW)	P_{Load} (MW)	Q_{Load} (MVar)	Q_{Cap} (MVar)
1(Slack)				
2	SG ₂ and WT#2 = 700			
3	SG ₃ = 719			
4	SG ₄ and WT#1 = 700			
7		$P_1 = 967$	$Q_1 = 100$	$Q_{C1} = 200$
8				$Q_{C3} = 125$
9		$P_2 = 1767$	$Q_2 = 100$	$Q_{C2} = 350$

Abbreviations: WT, wind turbine; SG, synchronous generators.

TABLE 5 Simulation cases.

Case	Description
1	Without WT and BESS
2	With WT#1 and without BESS
3	With WT#1 and WT#2 and without BESS
4	With WT#1, WT#2, and optimal BESS

Abbreviations: BESS, battery energy storage systems; WT, wind turbine.

4.1.1 | Case 1: Network without WT and BESS

In Figures 12 and 13, the frequency and voltage behaviours are depicted, respectively. As can be seen, after 13% decrease in SG₁ production, the voltage and frequency oscillation are still in allowable ranges (according to Table 2).

4.1.2 | Case 2: Network with 1 WT and without BESS

In this case, WT#1 is added, that is, the SG₄ is replaced by this WT. Then, the frequency and voltage stability of the network is evaluated with 13% decrease in SG₁ production as shown

in Figures 14 and 15, respectively. According to these figures, with the increase of WT penetration, the frequency of the network becomes unstable, that is, It is less than 49.6 for more than 5 min, due to the reduced inertia caused by increased penetration of renewable energy.

4.1.3 | Case 3: Network with 2 WTs and without BESS

In this scenario, WT#2 is also added to the network, that is, the SG₂ is also replaced by a WT; so, two WTs are existing in the network. Similar to cases 1 and 2, the frequency and voltage stability of the network is evaluated against 13% decrease in SG₁ production. The frequency and voltage stability are illustrated in Figures 16 and 17, respectively. It is obvious that with the increased penetration of WTs, the frequency is more unstable compared to Case 2. In terms of voltage for bus 6 and 7 violations of allowable range (out of the $\pm 2\%$) with the duration of 30 s and since this duration is less than 5 min the network voltage is still stable.

4.1.4 | Case 4: Network with Two WT and optimal BESS

To stabilize the network, the optimization approach presented in Section 3 has been carried out which result in optimal location, size and control parameters of BESS as listed in Table 6.

Considering Figures 18 and 19, with addition of the optimal BESS, in the event of 13% decrease in SG₁ production, the voltage and frequency fluctuations with two WTs are within the permissible ranges and compared to case 3 (Figures 16 and 17), they have returned to the stable conditions.

The frequency nadir and RoCoF values for cases 1 to 4 are reported in Table 7. According to this table, by increasing the WT penetration (cases 2 and 3) the frequency nadir is decreased while in case 4 it is increased due to active power injection

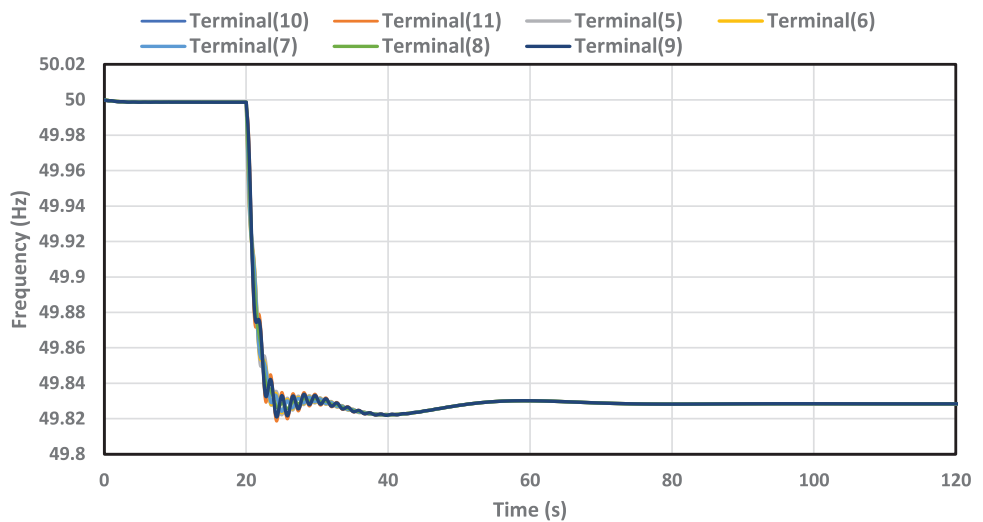


FIGURE 12 Frequency variation in case 1.

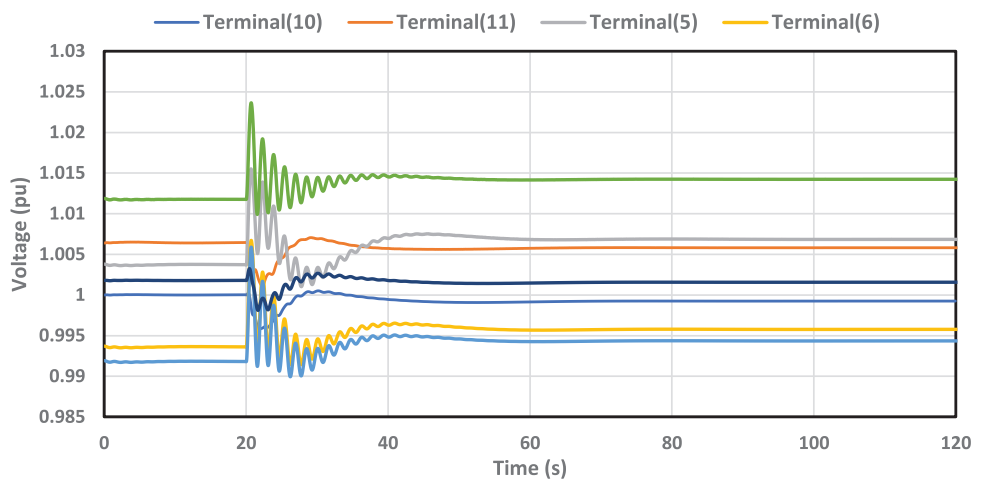


FIGURE 13 Voltage variation in case 1.

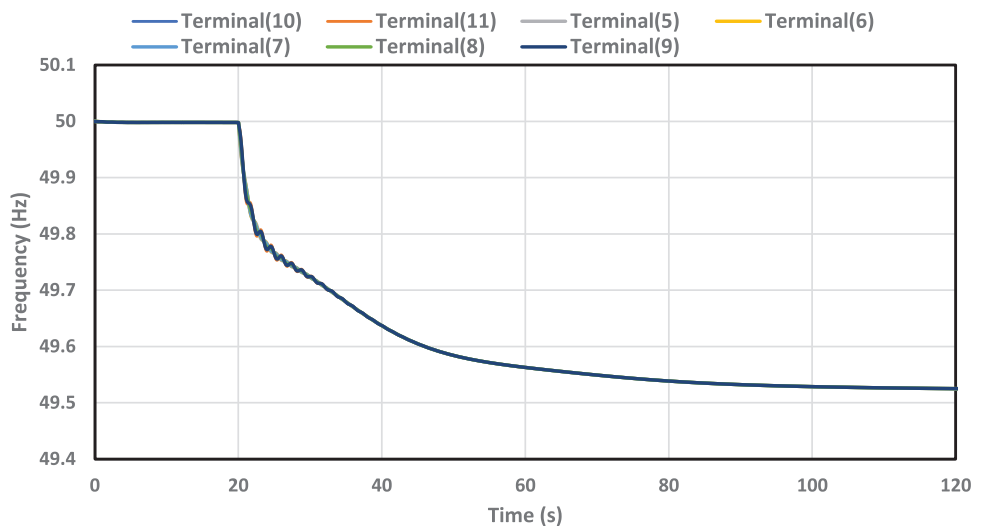


FIGURE 14 Frequency stability in case 2.

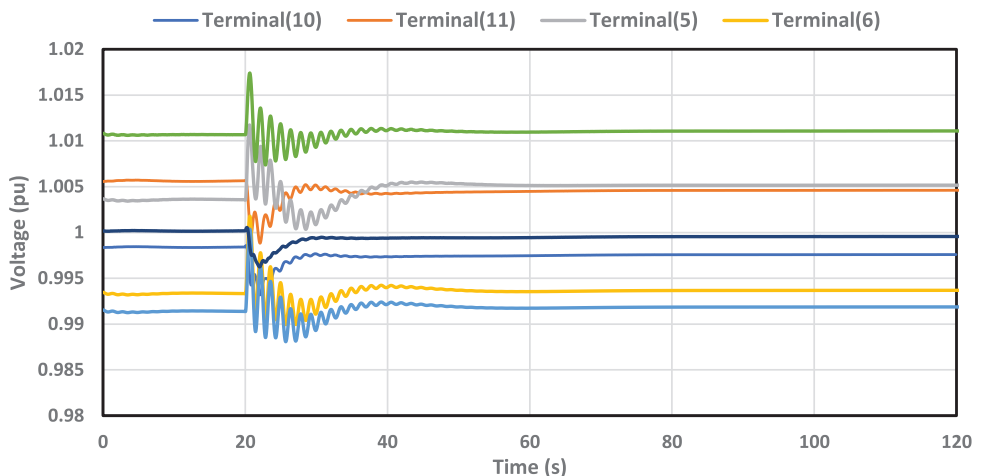


FIGURE 15 Voltage stability in case 2.

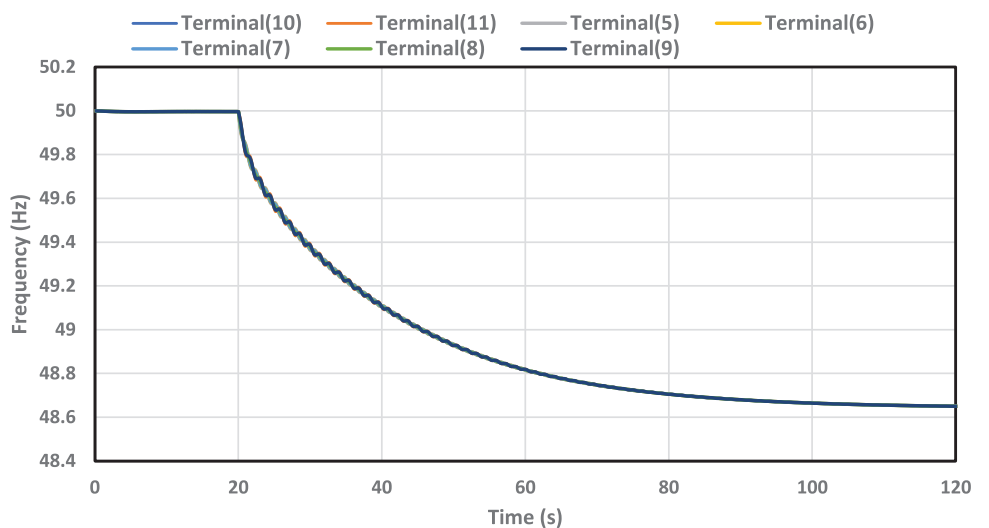


FIGURE 16 Frequency stability in case 3.

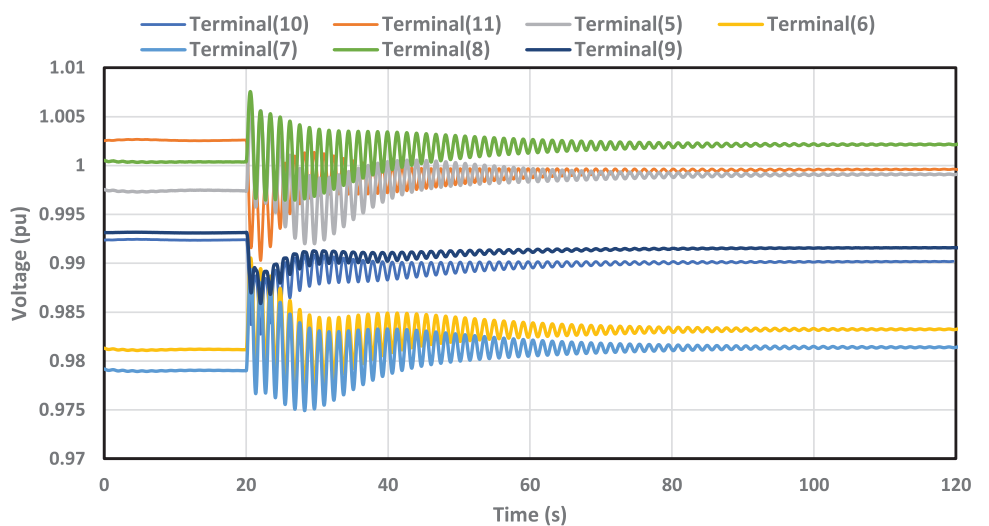


FIGURE 17 Voltage stability in case 3.

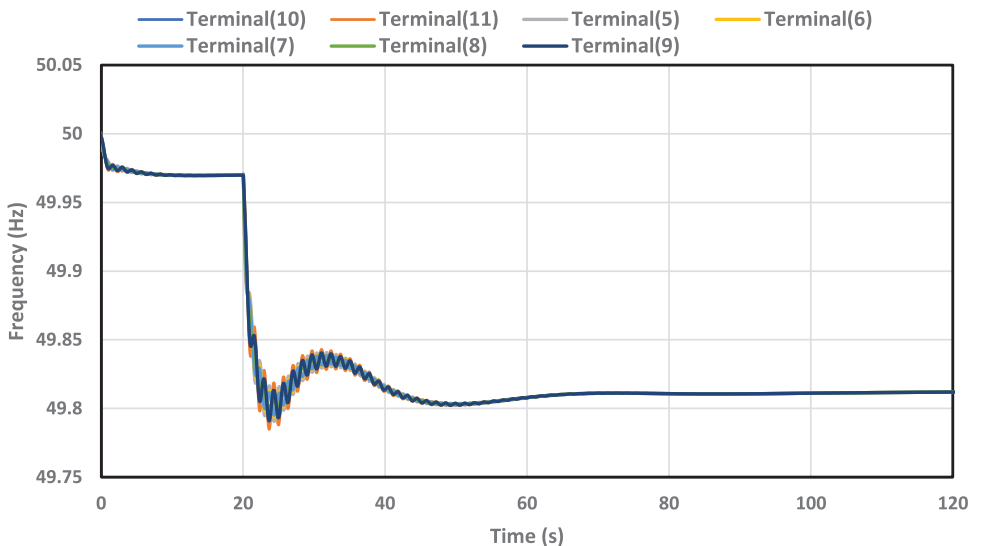


FIGURE 18 Frequency stability in case 4.

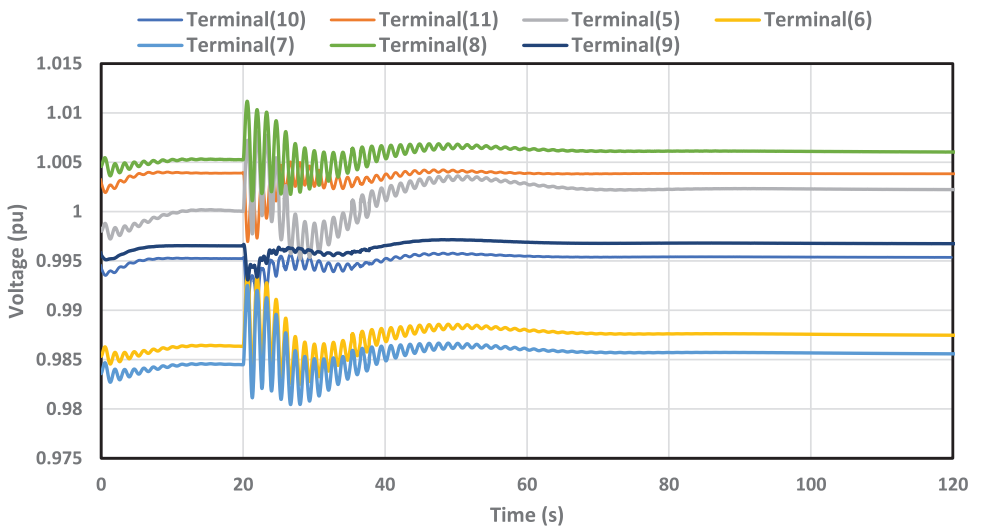


FIGURE 19 Voltage stability in case 4.

TABLE 6 Optimal battery energy storage system.

Location	Bus 5
Size	60 MW
Control parameters	
Tr	0.03
Trq	0.1
Kp	6.
Tip	0.001
Kq	1.
Tiq	0.000001
Kd	0.002
Dead band	0.0001

TABLE 7 Simulation cases.

Case	Frequency nadir (Hz)	RoCoF (Hz/s)
1	49.82	0.005
2	49.52	0.005
3	48.64	0.007
4	49.79	0.006

Abbreviation: RoCoF, rate of change of frequency.

by BESS. Although the RoCoF is not changed in case 2, it is increased in case 3 due to inertia reduction. In case 4, the RoCoF is decreased in comparison to case 3 due to BESS usage.

As an example, to compare cases 1 to 4, the frequency and voltage curves of Bus 8 are shown in Figures 20 and 21. As

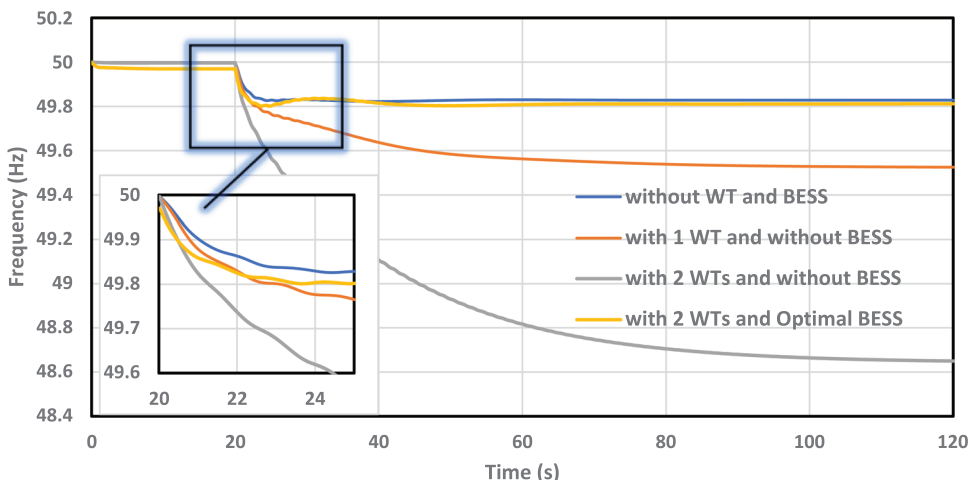


FIGURE 20 Frequency stability in cases 1 to 4 for Bus 8. BESS, battery energy storage systems; WT, wind turbine.

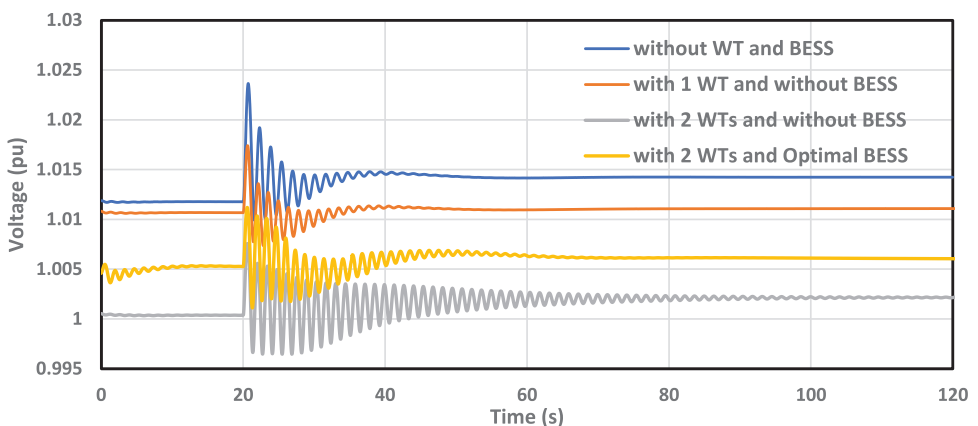


FIGURE 21 Voltage stability in cases 1 to 4 for Bus 8. BESS, battery energy storage systems; WT, wind turbine.

can be seen, with increasing WT penetration, the frequency becomes unstable while by optimal BESS addition, it returns to the allowable range. On the other hand, with two WTs, the voltage is stable for bus 8 and with optimal BESS voltage fluctuation is decreased.

In Figure 22, the active and reactive power injection by BESS is illustrated. When SG₁ production decreases as reflected by the frequency drop in Figures 14 and 16, the active power of the BESS increases to compensate the lack of production.

4.2 | IEEE 39-bus network

The studied network for this case study, that is, IEEE 39-bus network, is shown in Figure 23 [22]. Considering that in Section 4.1, the effect of adding WT and BESS on grid frequency and voltage stability was analysed in detail, in this section, the effectiveness of the proposed optimization method for placing, sizing and determining the optimal control parameters of the BESS in a larger network with more buses (39 buses) has been

evaluated. In other words, only a case similar to the case 4 of Section 4.1 has been investigated.

As a first step, in the bus 23 a WT with a power of 560 MW has replaced the synchronous generator G07. Then, by taking into account 15% reduction in generator power production of G04 in bus 33, the voltage and frequency stability of the network has been shown in the Figure 24. It should be noted that in IEEE 39-bus network, the nominal frequency is 60 Hz. By assuming that allowed range of frequency is ± 0.2 Hz, it can be seen that the network frequency is out of the allowed range for stability.

Then, utilizing the optimization method proposed in this paper, the optimal placement, sizing and parameters of BESS have been determined to overcome the stability challenge experienced by this network. Table 8 lists the size, location and optimal parameters of the BESS.

In Figure 24, the stability of frequency after installing the optimal BESS is demonstrated for bus 15.

As it can be seen, the frequency of the network has improved and is within the permissible range (i.e., frequency nadir is

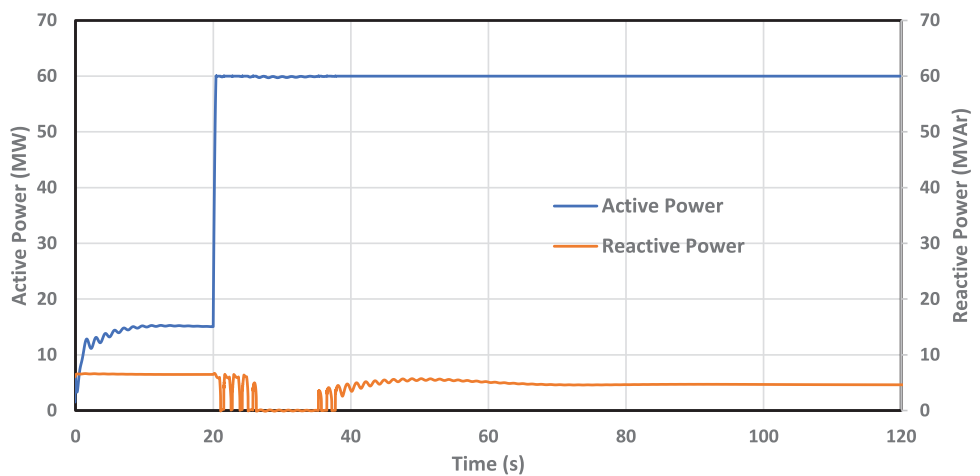


FIGURE 22 Active and reactive power of optimal battery energy storage systems.

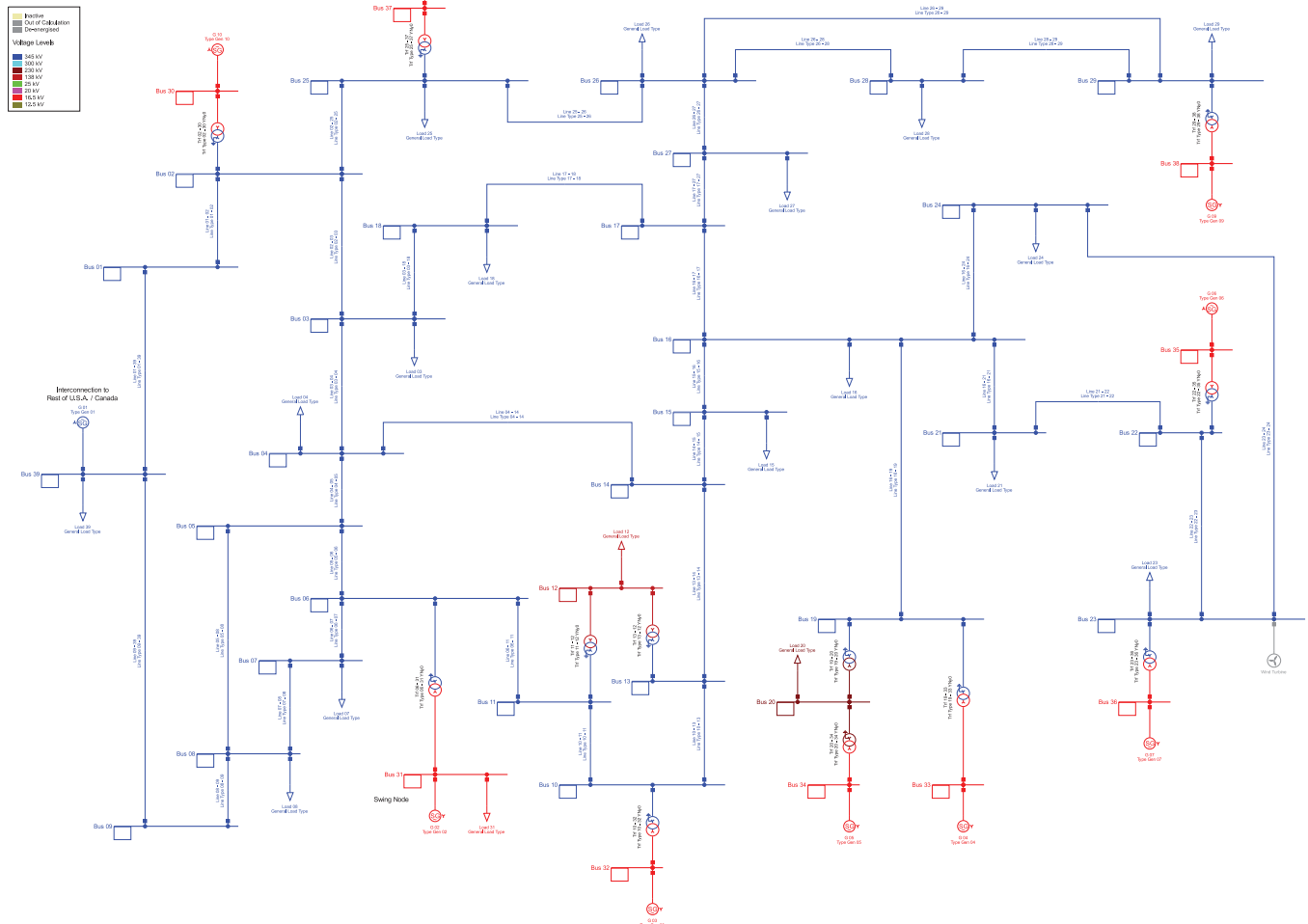


FIGURE 23 IEEE 39-bus network.

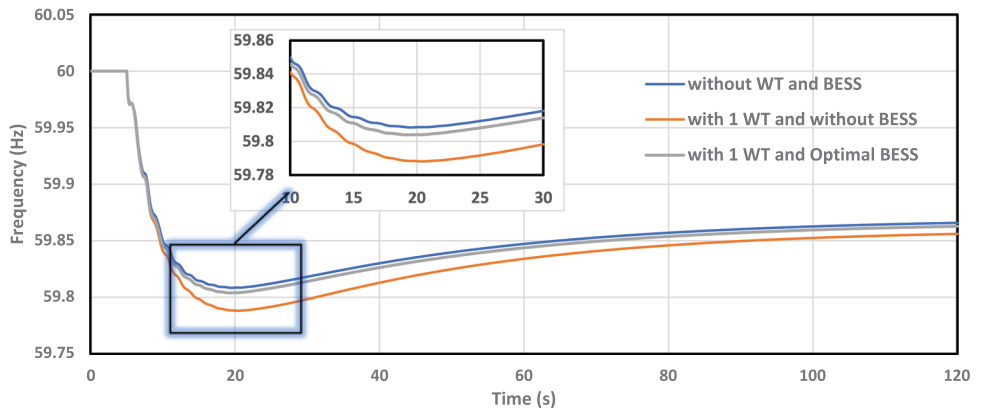


FIGURE 24 Frequency stability of bus 15 in IEEE 39 bus. BESS, battery energy storage systems; WT, wind turbine.

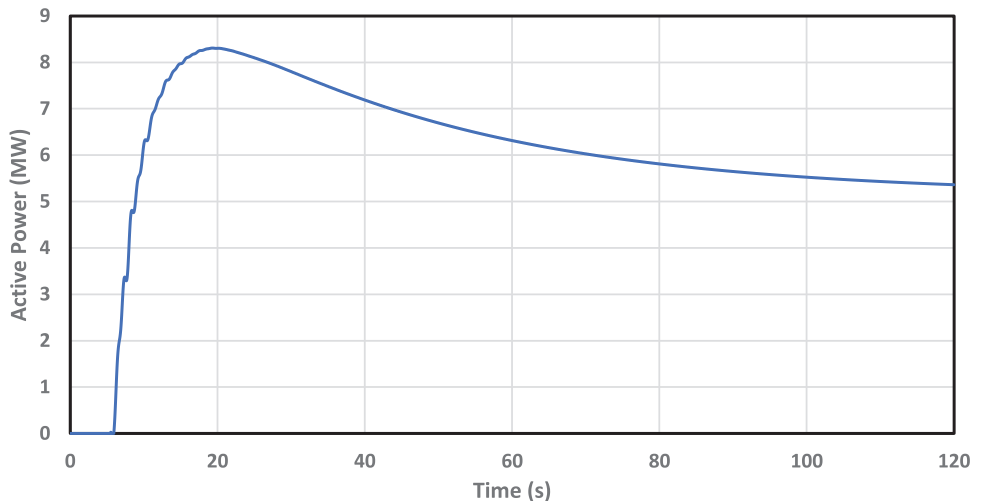


FIGURE 25 Active power of optimal battery energy storage systems.

TABLE 8 Optimal battery energy storage systems.

Location	Bus 05
Size	9 MVA
Control parameters	
Tr	0.04
Trq	0.1
Kp	72
Tip	0.000001
Kq	2
Tiq	1
Kd	0.003
Dead band	0.0005

increased). In Figure 25 the amount of active power injected by the BESS at the time of generator power reduction has been shown. As can be seen, at the moment of the loss of generation event, the BESS restores the frequency nadir by injecting active power.

In order to highlight the impact of the proposed approach for optimization of control parameters two scenarios are considered. One with the optimized parameters using our approach and in the other, instead of optimizing the control parameters, the parameters values of [22] have been used. Then the frequency stability of bus 15 is evaluated for these two sets control parameters. As can be seen in Figure 26 that without optimal control parameter the frequency nadir is decreased.

For validation, only the impact of optimized control parameters have been examined, similar evaluation can be performed for sizing and location of BESS.

5 | CONCLUSION

As seen, with the increase of WT penetration due to the reduction of network inertia, the stability of network's voltage and frequency is affected, that is, RoCoF and frequency nadir are increased and decreased, respectively. To optimize BESS, an objective function with three terms was considered, which included the active power of the BESS, RoCoF and RFN. The constraints for frequency and voltage were set to ± 0.2 Hz and

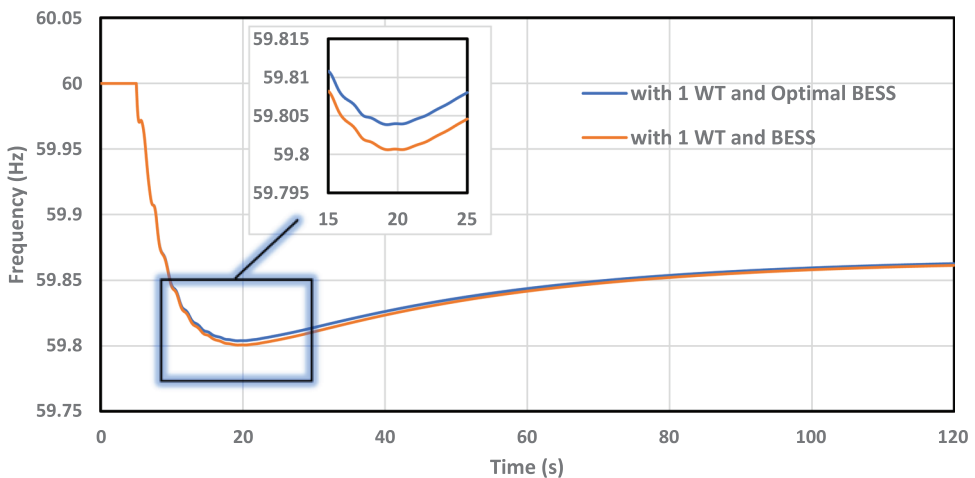


FIGURE 26 Frequency stability of bus 15 to validate proposed method. BESS, battery energy storage systems; WT, wind turbine.

$\pm 2\%$, respectively. This objective function was optimized using the GA which in each population, the location, size, and control parameters of BESS were considered simultaneously. Considering that the investigated disturbance is the reduction of active power production, affects the frequency more and leads to frequency instability, while the network does not experience voltage instability. It has been demonstrated that when the generation of one of the SGs was reduced, the optimal BESS could contribute to the enhancement of frequency and voltage stability. In present paper, the frequency control was only done by a conventional simple control for WTs and instead a simple BESS take over the role of stabilization. It could also be done by more complicated control of WTs for example in grid forming operation such as virtual inertia emulation. Such implementation and coordination for WTs and BESS for such operation will be investigated in our future work. Also grid following control of WTs with frequency and voltage support services could help. Finally, the investigation of large-signal or transient stability can be evaluated in future works.

AUTHOR CONTRIBUTIONS

Mohammad Rasol Jannesar: Conceptualization; formal analysis; investigation; methodology; resources; software; writing—original draft. **Sajad Sadr:** Investigation; project administration; resources; writing—original draft. **Mehdi Savaghebi:** Conceptualization; investigation; resources; supervision; validation; writing—review and editing.

ACKNOWLEDGEMENTS

This work has been supported by the Center for International Science Studies & Collaboration (CISSC), Ministry of Science, Research and Technology.

CONFLICT OF INTEREST STATEMENT

The authors declare no conflicts of interest.

DATA AVAILABILITY STATEMENT

Data available on request from the authors.

ORCID

Mohammad Rasol Jannesar <https://orcid.org/0000-0002-3126-1073>

Mehdi Savaghebi <https://orcid.org/0000-0001-6188-0265>

REFERENCES

1. Muftau, B., Fazeli, M.: The role of virtual synchronous machines in future power systems: A review and future trends. *Electr. Power Syst. Res.* 206, 107775 (2022)
2. IRENA: Renewable Power Generation Costs in 2021. IRENA, Abu Dhabi (2022)
3. Renewable capacity highlights. IRENA, Abu Dhabi. https://www.irena.org/-/media/Files/IRENA/Agency/Publication/2022/Apr/IRENA_-RE_Capacity_Highlights_2022.pdf (2022). Accessed 12 May 2024.
4. Deguenon, L., Yamegueu, D., kadri, S.M., Gomna, A.: Overcoming the challenges of integrating variable renewable energy to the grid: A comprehensive review of electrochemical battery storage systems. *J. Power Sources*. 580, 233343 (2023)
5. Ratnam, K.S., Palanisamy, K., Yang, G.: Future low-inertia power systems: Requirements, issues, and solutions—A review. *Renewable Sustainable Energy Rev.* 124, 109773 (2020)
6. Machowski, J., Bialek, J.W., Bumby, D.J.: *Power System Dynamics: Stability and Control*, 2 ed. John Wiley & Sons, Hoboken, NJ (2011)
7. Kundur, P.: *Power System Stability and Control*. McGraw-Hill Education, New York (1994)
8. Shair, J., Li, H., Hu, J., Xie, X.: Power system stability issues, classifications and research prospects in the context of high-penetration of renewables and power electronics. *Renewable Sustainable Energy Rev.* 145, 111111 (2021)
9. Remon, D., Cantarella, A.M., Mauricio, J.M., Rodriguez, P.: Power system stability analysis under increasing penetration of photovoltaic power plants with synchronous power controllers. *IET Renewable Power Gener.* 11(6), 733–741 (2017)
10. Shah, R., Mithulanthan, N., Bansal, R.C., Ramachandaramurthy, V.K.: A review of key power system stability challenges for large-scale PV integration. *Renewable Sustainable Energy Rev.* 41, 1423–1436 (2015)
11. Mosca, C., et al.: Mitigation of frequency stability issues in low inertia power systems using synchronous compensators and battery energy storage systems. *IET Gener. Transm. Distrib.* 13(17), 3951–3959 (2019)
12. Dreidy, M., Mokhlis, H., Mekhilef, S.: Inertia response and frequency control techniques for renewable energy sources: A review. *Renewable Sustainable Energy Rev.* 69, 144–155 (2017)
13. Niu, D., Fang, J., Yau, W., Goetz, S.M.: Comprehensive evaluation of energy storage systems for inertia emulation and frequency regulation improvement. *Energy Rep.* 9, 2566–2576 (2023)

14. Siqueira, L.M.S.d., Peng, W.: Control strategy to smooth wind power output using battery energy storage system: A review. *J. Energy Storage* 35, 102252 (2021)
15. Rana, M.M., Uddin, M., Sarkar, M.R., Shafiullah, G.M., Mo, H., Atef, M.: A review on hybrid photovoltaic—Battery energy storage system: Current status, challenges, and future directions. *J. Energy Storage* 51, 104597 (2022)
16. Shazon, M.N.H., Nahid-Al-Masood, H.M.A., Deeba, S.R., Hossain, E.: Exploring the utilization of energy storage systems for frequency response adequacy of a low inertia power grid. *IEEE Access* 9, 129933–129950 (2021)
17. Datta, U., Kalam, A., Shi, J.: The relevance of large-scale battery energy storage (BES) application in providing primary frequency control with increased wind energy penetration. *J. Energy Storage* 23, 9–18 (2019)
18. Adrees, A., Milanović, J.V., Mancarella, P.: The influence of location of distributed energy storage systems on primary frequency response of low inertia power systems. In: Proceedings of the IEEE Power & Energy Society General Meeting (PESGM), pp. 1–5. IEEE, Piscataway, NJ (2018)
19. Aluthge, C.D., Hemapala, K.T.M.U., Lucas, J.R.: Using BESS to achieve power system dynamic stability when high solar penetration is present: Case study Sri Lanka. In: Proceedings of the 2nd International Conference on Smart Power & Internet Energy Systems (SPIES), pp. 252–257. IEEE, Piscataway, NJ (2020)
20. Jannesar, M.R., Sadr, S., Savaghebi, M.: Dynamic stability enhancement in low-inertia power systems using battery energy storage. In: Proceedings of the 12th Smart Grid Conference (SGC), pp. 1–5. IEEE, Piscataway, NJ (2022)
21. Alsharif, H., Jalili, M., Hasan, K.N.: Power system frequency stability using optimal sizing and placement of battery energy storage system under uncertainty. *J. Energy Storage* 50, 104610 (2022)
22. Ramos, A.F., Ahmad, I., Habibi, D., Mahmoud, T.S.: Placement and sizing of utility-size battery energy storage systems to improve the stability of weak grids. *Int. J. Electr. Power Energy Syst.* 144, 108427 (2023)
23. Farmer, W.J.: Optimising power system frequency stability using virtual inertia from inverter-based renewable energy generation. Master Thesis, University of Stellenbosch (2019)
24. User Manual. DIgSILENT PowerFactory (2022). <https://www.digsilent.de/en/downloads.html>. Accessed 1 May 2024
25. Gusain, D.: Parameter identification of dynamic equivalents for active distribution systems using heuristic optimisation techniques. Master Thesis, Delft University of Technology (2016)
26. Gonzalez-Longatt, F.M., Torres, J.L.R.: Modelling and Simulation of Power Electronic Converter Dominated Power Systems in PowerFactory. Springer, Berlin (2021)
27. DIgSILENT PowerFactory: Battery Energy Storing Systems. DIgSILENT PowerFactory, Gomaringen, Germany (2010)
28. Operating instructions of Iran's electricity network. <https://www.igmc.ir/Documents?EntryId=275634>. Accessed 1 May 2024
29. Saeedian, M., Eskandari, B., Taheri, S., Hinkkanen, M., Pouresmaeil, E.: A control technique based on distributed virtual inertia for high penetration of renewable energies under weak grid conditions. *IEEE Syst. J.* 15(2), 1825–1834 (2021)
30. Blaabjerg, F.: Control of Power Electronic Converters and Systems. Elsevier Science, Amsterdam (2021)
31. Mohssine, C., Nasser, T., Essadki, A.: Contribution of variable speed wind turbine generator based on DFIG using ADRC and RST controllers to frequency regulation. *Int. J. Renewable Energy Res.* 11(1), 320–331 (2021)
32. Kenyon, R.W., et al.: Stability and control of power systems with high penetrations of inverter-based resources: An accessible review of current knowledge and open questions. *Sol. Energy* 210, 149–168 (2020)
33. Preece, R.: Improving the Stability of Meshed Power Networks. Springer, Berlin (2013)

How to cite this article: Jannesar, M.R., Sadr, S., Savaghebi, M.: Optimal siting, sizing and control of battery energy storage to enhance dynamic stability of low-inertia grids. *IET Renew. Power Gener.* 18, 2925–2941 (2024). <https://doi.org/10.1049/rpg2.13079>

APPENDIX

In this appendix, according to the PowerFactory model, the details of modelling governor and AVR for SG and PQ and the current controller for WT are provided.

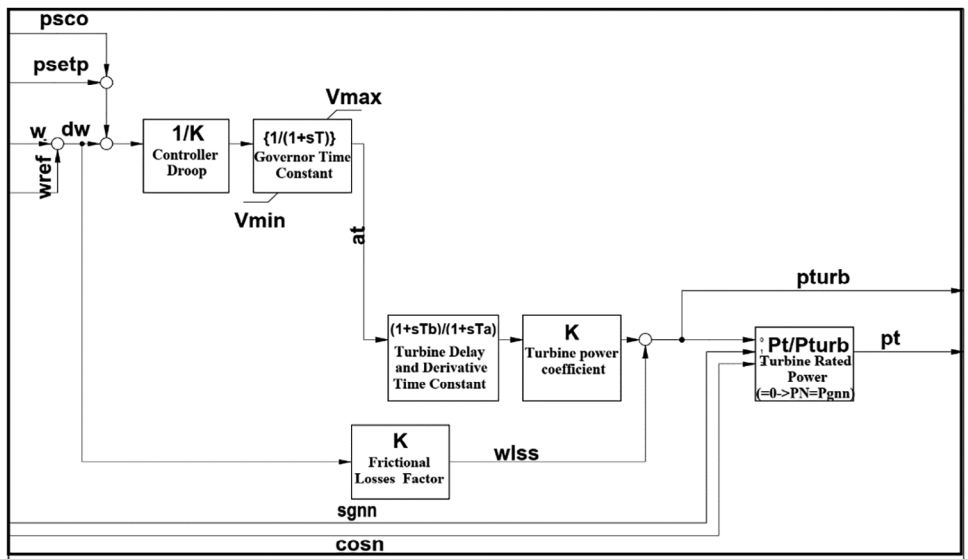


FIGURE A1 Block diagram of governor.

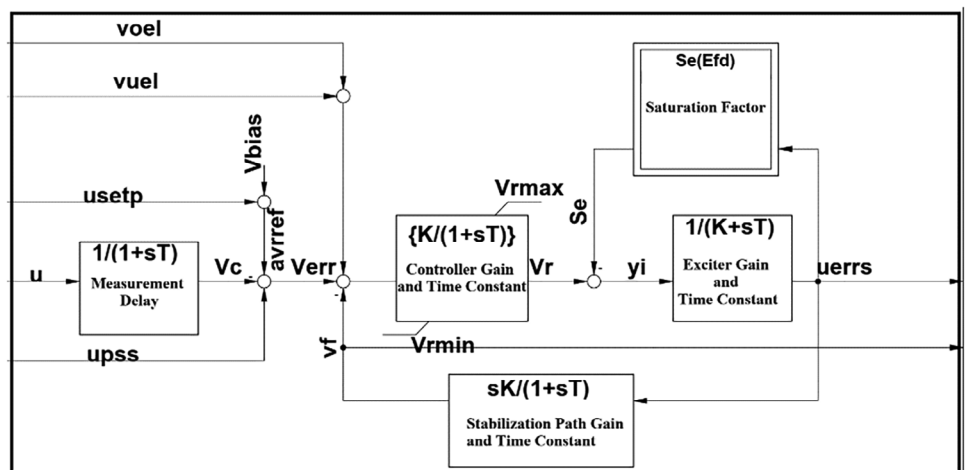


FIGURE A2 Block diagram of automatic voltage regulator.

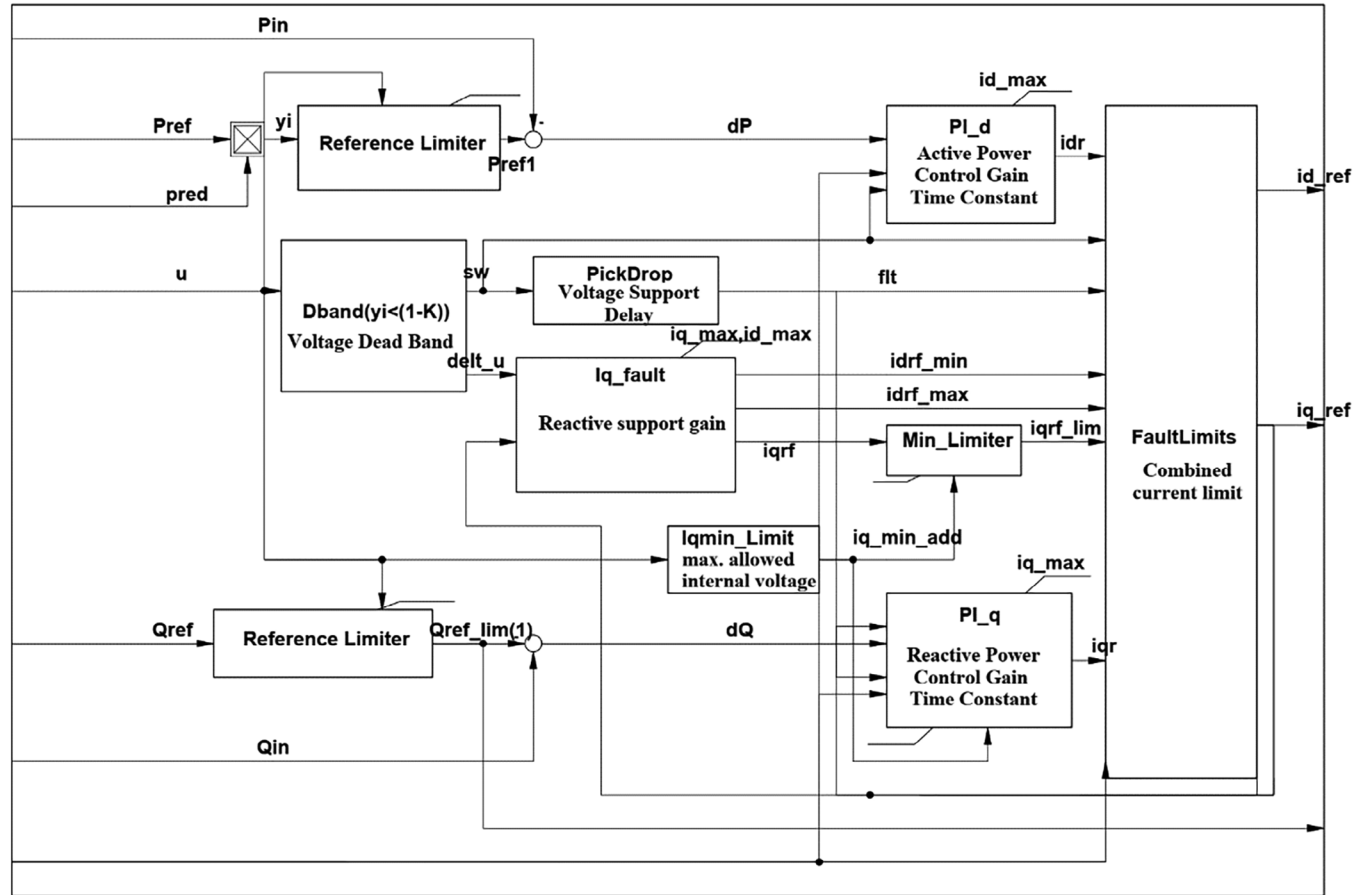


FIGURE A3 Block diagram of PQ controller.

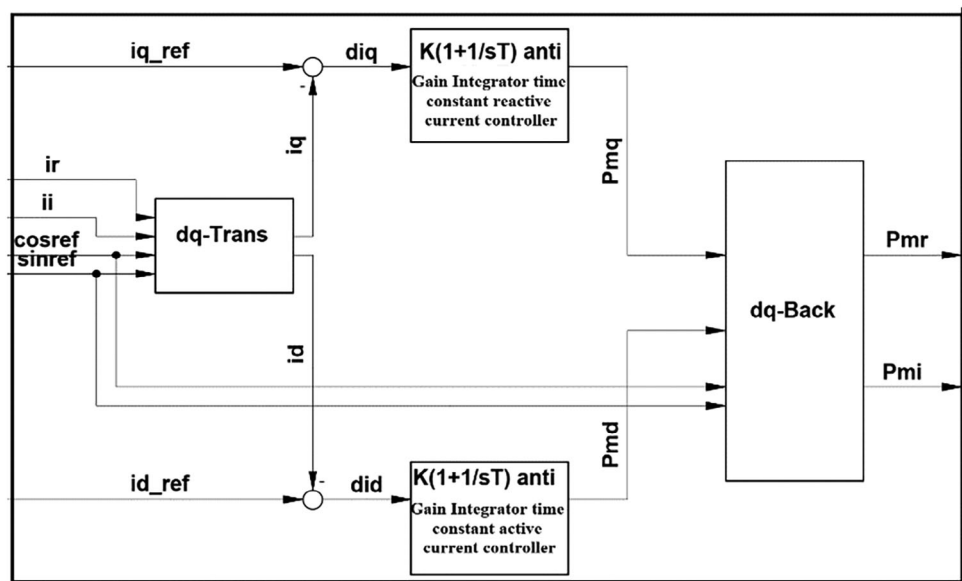


FIGURE A4 Block diagram of current controller.